Journal of Alloys and Compounds 629 (2015) 332–342

Contents lists available at ScienceDirect

Journal of Alloys and Compounds

journal homepage: www.elsevier.com/locate/jalcom

Magnetocaloric effect, magnetostructural and magnetic phase transformations in $Ni_{50.3}Mn_{36.5}Sn_{13.2}$ Heusler alloy ribbons

R. Caballero-Flores [a,*], L. González-Legarreta [a], W.O. Rosa [b], T. Sánchez [a], V.M. Prida [a], Ll. Escoda [c], J.J. Suñol [c], A.B. Batdalov [d], A.M. Aliev [d], V.V. Koledov [e], V.G. Shavrov [e], B. Hernando [a]

[a] Dpto. de Física, Universidad de Oviedo, Calvo Sotelo s/n, 33007 Oviedo, Spain
[b] Centro Brasileiro de Pesquisas Físicas, CEP 22290-180 Urca, Rio de Janeiro, Brazil
[c] Universidad de Girona, Campus Montilivi (Ed. PII), Lluís Santaló s/n, 17003 Girona, Spain
[d] Amirkhanov Institute of Physics of Daghestan Scientific Center, RAS, Makhachkala 367003, Russia
[e] Kotelnikov Institute of Radio Engineering and Electronics, RAS, Moscow 125009, Russia

ARTICLE INFO

Article history:
Received 17 October 2014
Received in revised form 13 December 2014
Accepted 15 December 2014
Available online 24 December 2014

Keywords:
Heusler alloys
Magnetocaloric effect
Martensitic transformation
Magnetic properties
Phase transitions

ABSTRACT

Thermomagnetic properties and magnetocaloric effect (MCE) in $Ni_{50.3}Mn_{36.5}Sn_{13.2}$ Heusler alloy ribbons are reported. Large magnetocaloric response has been obtained for $\mu_0 H = 3$ T in both the reversible adiabatic change in temperature ΔT_{ad} (−6.3 and +4.7 K) and the isothermal change in the total entropy ΔS_T (+11.8 and −2.2 J K^{-1} kg^{-1}), respectively at the temperature $T_{str} = 271$ K at which the magnetostructural phase transition from the low-temperature Martensite phase (MP) to the high-temperature Austenite phase (AP) takes place, and at $T_{CA} = 311$ K at which the magnetic phase transition in the AP occurs. The MCE has been studied through the Stoner's magnetocaloric parameter ξ_S (Stoner EC. Phil Mag 19 (1935) 565), and a generalized expression for the equations of state for magnetic materials is presented. The phase coexistence of the MP and AP has been studied via their respective sublattice with opposite-aligned magnetic moments by means of the effective magnetic anisotropy density e_A induced by the supercooled (superheated) secondary AP (MP) in the MP (AP). Magnetic fields higher than the critical value of $\mu_0 H_R = 0.5$ T produce alignment of the two magnetic moments and hence a change in the magnetic ordering in the MP from antiferromagnetic to ferromagnetic, resulting in a thermomagnetic behavior in which the field-cooling and field-heating magnetizations become coincident, the induced anisotropy vanishes $e_A = 0$ and the metastability disappears. New tentative methods to obtain the spontaneous magnetization of both MP and AP and their respective fractions in the phase coexistence range are reported.

1. Introduction

The magnetocaloric effect (MCE), which consists of the heating or the cooling of magnetic solids in a varying magnetic field, has the potential to offer an environmentally green saving and an enhancement in the energy efficiency over conventional room-temperature refrigeration techniques based on the compression/expansion of gases [1,2]. The applied importance of the MCE is easily proved since it has been successfully used to reach, for the first time, ultra-low temperatures (<1 K) [3].

The MCE is characterized by the reversible adiabatic change in temperature ΔT_{ad}, or by the isothermal change in entropy ΔS_T, underwent by a magnetic material when subjected to an external magnetic field change ΔH [4]. The thermodynamic coefficients that control this process can be expressed, in a first-order approximation, as a function of the dimensionless Stoner's magnetocaloric parameter ξ_S [5]: being $dT_{ad} = (\partial T/\partial H)_S dH = T d\xi_S$ and $dS_T = (\partial S/\partial H)_T dH = -C_H d\xi_S$, or the relations between them $dT_{ad} = -(T/C_H) dS_T$ and $dS_T dT_{ad} = -(T/C_H)(dS_T)^2 = -(C_H/T)(dT_{ad})^2$, where $C_H = T(\partial S/\partial T)_H$ is the heat capacity at constant H. The higher the magnetocaloric parameter $d\xi_S$ values, the higher dT_{ad} and dS_T ones (in absolute value).

The figure of merit of the MCE is the so-called refrigerant capacity defined as $d\eta = \Delta T_{ad} dS$ or $d\eta = \Delta S_T dT$ that integrated over the S or T spans in the S–T region where the MCE exists, provides the amount of heat η that can be transferred between the hot and cold reservoirs of the thermodynamic cycle. Since ΔT_{ad} is more difficult to measure experimentally than ΔS_T, the latter second equation is usually employed and the temperature span is defined, by convenience, as the temperature range spanning the half-maximum of the $\Delta S_T(T)$ curve [6].

* Corresponding author.
E-mail address: rafaelcaballero@us.es (R. Caballero-Flores).

http://dx.doi.org/10.1016/j.jallcom.2014.12.099
0925-8388/

According to the experimental research, while the largest ΔT_{ad} or ΔS_T values have been achieved in materials with first-order phase transitions (FOPT) (within the Ehrenfest classification [7]), the temperature and entropy spans in which the MCE occurs are higher in materials with second-order phase transitions (SOPT) what, in general, can result in an enhancement of the refrigerant capacity η [8–11]. Consequently, research in magnetic refrigeration has therefore focused on exploring new magnetocaloric materials and novel strategies that maximize the MCE by increasing the value of ΔS_T or ΔT_{ad}, and/or broadening the temperature or entropy spans over which the magnetocaloric response takes place, thereby increasing the refrigerant capacity η [12–15] (see Ref. [10] and references therein).

Heusler alloys based on Ni–Mn–Z (Z = In, Sn or in general a group IIIA–VA element) have been recently presented as an important class of magnetocaloric materials for enhancing ξ_S in both the direct ($\Delta T_{ad} > 0$ or $\Delta S < 0$) and inverse ($\Delta T_{ad} < 0$ or $\Delta S > 0$) MCE [16–21]. These intermetallic compounds may undergo the following consecutive phase transitions: a magnetic SOPT that takes place at temperature T_{CM} in the low-temperature Martensite phase (MP); followed by a magnetostructural FOPT from the low-temperature MP to the high-temperature Austenite phase (AP) at the temperature T_{str}, involving a change in both structural (exhibiting in general a noticeable increase in the lattice parameters in the AP) and magnetic (commonly a significant increase in the spontaneous magnetization M_0 in the AP) properties of the material; and a second magnetic SOPT in the high-temperature AP that occurs at the temperature T_{CA}. The difference between the critical temperature values at which these phase transitions occur is an important feature exhibited by these compounds. In this work the sequence of these temperatures results $T_{CM} < T_{str} < T_{CA}$.

Within the Ehrenfest scheme, the overheating (undercooling) of the MP (AP) arises naturally in the FOPT but neither their temperature and field limits nor metastable nature are specified. The existence of these overheating and undercooling gives rise to the thermal and magnetic hystereses of any thermodynamic variable *Y*. A phase-coexistence of a high-temperature metastable AP and a low-temperature equilibrium MP, and *vice versa*, is also another consequence of this FOPT. This MP–AP phase coexistence or metastability must be taken into account in order to study the thermomagnetic properties of these compounds.

According to the literature, in the intermetallic $Ni_{50}Mn_{25}Sn_{25}$ compounds the magnetic moments are located at the Mn sites with a ferromagnetic (FM) exchange interaction in both the MP and AP phases [22]. On the other hand, as part of Sn content is replaced by Mn in $Ni_{50}Mn_{25+x}Sn_{25-x}$, the excess of Mn atoms occupy Sn sites reducing the Mn–Mn stoichiometric ($x = 0$) distance that, together with the reduction of the lattices parameters, make the antiferromagnetic (AFM) exchange arises in the MP, located in the environment of the Mn ions at both the Mn and Sn sites [23,24].

The aim of this work is to study the magnetic and magnetostructural phase transitions and their influences on the thermomagnetic and magnetocaloric (ΔT_{ad} and ΔS_T) behaviors of $Ni_{50.3}Mn_{36.5}Sn_{13.2}$ Heusler alloys. The dimensionless Stoner's magnetocaloric parameter ξ_S has been introduced in order to study the MCE in a more compact way, and a generalized expression for the equations of state for magnetic materials will be shown. Our study of the FOPT (MP ↔ AP) below and above the transition temperature T_{str} at which takes place, provides deeper insights into the influence of the AP–MP phase coexistence on the magnetic properties of the studied Heusler alloy ribbons. A better understanding of the temperature and field limits of the phase coexistence and its metastable nature will be shown. The strong temperature dependence of the magnetic permeability (μ) in the MP due to the effective magnetic anisotropy density e_A induced by the secondary AP still remaining, has turned out to be the cause of the Quasi-Diamagnetic-like (QD) behavior and the compensation point T_{cp} at which the magnetization *M* vanishes, present in this kind of compounds. Magnetic fields higher than the critical value $\mu_0 H_R = 0.5$ T produce alignment of the two magnetic moments in the MP and AP phases in the studied $Ni_{50.3}Mn_{36.5}Sn_{13.2}$ Heusler alloy ribbons, resulting in a change in the magnetic ordering in the MP from AFM to FM, and a thermomagnetic behavior in which the field-cooling and field-heating magnetizations become coincident, the induced anisotropy vanishes $e_A = 0$ and the metastability disappears.

At the same time, our study of the SOPT that undergoes the AP by means of its critical exponents and the universal behaviors of *M* and its relation with the MCE, will allow us to assume the long- and short-range type magnetic interactions in the AP and MP phases, respectively as well as to obtain the *spontaneous magnetization* M_0 of both phases beyond the metastability range ($H > H_R$). New tentative method to obtain the respective fractions of the MP and AP in the phase coexistence range will be reported.

2. Experimental details

Starting from high-purity metallic-constituent elements (>99.98%), a polycrystalline $Ni_{50}Mn_{25+x}Sn_{25-x}$ ($x = 11.5$) alloy ingot was prepared by conventional arc melting method under pure argon gas atmosphere. Thereupon the excess-Mn polycrystalline ribbons were obtained by means of the melt-spinning technique, also in a purified argon atmosphere, ejecting the previously induction-arc-melted sample in a quartz tube onto the polished surface of a copper wheel rotating at the high linear speed of 48 m/s. The phase and crystal structure was determined by X-ray diffraction (XRD), measured at Diamond Light Source Synchrotron (I16—Materials and Magnetism Beamline), below (at 100 K < T_{CM}) and above (at 340 K > T_{CA}) the existing phase transition temperatures by using Cu Kα radiation with wavelength of $\lambda = 1.127$ Å in the range $10° \leqslant 2\theta \leqslant 110°$.

The microstructure, as well as the elemental chemical composition analyses, were checked by means of Scanning Electron Microscopy (SEM, JEOL 6100) equipped with an Energy Dispersive X-ray microanalysis system (EDX, Inca Energy 200). From these analyses we obtain that: (i) SEM images from cross-section together with top and bottom ribbon surfaces show a highly oriented columnar-grain microstructure, in which the longer axis of individual grains is perpendicularly oriented to both ribbon surfaces; and, (ii) multiple EDX microanalyses indicate an accuracy of 0.1% of each element in the $Ni_{50.29}Mn_{36.47}Sn_{13.24}$ average composition with an excess of Mn $x = 11.50(4)$, and a valence electron concentration per atom $e/a = 8.11(1)$ (calculated as the concentration weighted sum of the number of 3*d* and 4*s* electrons of Ni and Mn, and the corresponding number of 5*s* and 5*p* of Sn).

The field (H) and temperature (T) dependence of the magnetization $M(T,H)$ of the ribbons were measured with a commercial Vibrating Sample Magnetometer (VSM-VersaLab). The magnetic field during the experiment was always applied along the ribbon plane in order to minimize the demagnetization effects [25].

The thermal hysteresis of the samples has been studied by means of the isofield magnetization curves $M_H(T)$, in the temperature range from 50 K to 400 K (in increments of 0.5 K) using zero-field cooling (ZFC), field-cooling (FC) and field-heating (FH) protocols. Prior to the ZFC measurements, the sample was prepared in a zero-field state by cooling it from 400 to 50 K, denoted as ZFC^{-} process. The cooling and heating rates in these measurements were 5 K/min.

The magnetic hysteresis has also been analyzed from the isothermal magnetization $M_T(H)$ measurements, by applying an external magnetic field up to $\mu_0 H = 3$ T in 10 mT increments, at the experimental temperature T_0 in the temperature range where the magnetostructural (at T_{str}) and magnetic (at T_{CA}) phase transitions take place after reaching these temperatures in two different protocols P1 and P2: in P1 the samples were zero-field cooled down to 50 K, heated up to the experimental temperature T_0, followed by the heating up to the next experimental temperature $T_0 + dT$, with a step of $dT = 1$ K; and in P2, the samples were also firstly zero-field cooled down to 50 K and heated up to T_0, with the difference that the next experimental temperature T_0 is reached when the zero-field cooling down to 50 K process is repeated, followed by the corresponding heating up to $T_0 + dT$ (with $dT = 1$ K).

The zero-field heat capacity $C(T,0)$ measurements were carried out using an a.c.-calorimeter by an adiabatic heat relaxation technique in the temperature range from 117 K to 340 K in 0.5 K step increments, encompassing both the magnetostructural and magnetic phase transformations presented in the studied system.

3. Determination of the magnetocaloric and thermomagnetic properties

3.1. Magnetocaloric effect

The magnetocaloric effect (MCE) is related to the physical phenomenon in which magnetic materials undergo an adiabatic

reversible change in temperature ΔT_{ad}, defined as $\Delta T_{ad}(T,H) = T(H) - T(0)$, when they are adiabatically subjected to an effective external magnetic field H (after appropriately corrected by the demagnetizating field) [1]. The field evolution of the temperature $T(H)$ in a magnetocaloric material with SOPT or continuous phase transitions is given by:

$$T(H) = T(0)\exp^{\xi_S}, \tag{1}$$

with the dimensionless Stoner's magnetocaloric parameter ξ_S:

$$\xi_S(T,H) = -\mu_0 \int_0^H (\partial M_{T,H}/C_H)dH, \tag{2}$$

where μ_0 is magnetic permeability of vacuum, M the net component of the magnetization parallel to H, $C(T,H) = C_H(T)$ the heat capacity at constant H, and $\partial M_{X,Y}$ the X-derivative of M at constant Y. The heat capacity can be analyzed considering additive and independent contributions from the magnetic $C_M(T,H)$, lattice $C_L(T,H)$ and, as a first approximation, field independent electronic $C_E(T)$ subsystems [26,27]. By convenience we assume an isobaric process at pressure P, and zero initial field has been considered ($\Delta H = H$).

Therefore:

$$\Delta T_{ad}(T,H) = T(0)(\exp^{\xi_S} - 1) \simeq T(0)\xi_S, \tag{3}$$

where the first-order Taylor series approximation of the exponential function has been used, as it is usually presented in the literature, permissible for ferromagnets in which the MCE becomes only appreciable at temperatures not very far from the phase transitions, but not for paramagnets near zero absolute value, where the heat capacity approaches to zero [5,28–31].

Alternatively, related to the adiabatic change in temperature ΔT_{ad}, when the magnetic materials are isothermally subjected to an applied magnetic field, there is an isothermal reversible change in the total entropy ΔS – we omit the subscript T in order to avoid confusions – given by the Maxwell relations [32]:

$$\Delta S(T,H) = \mu_0 \int_0^H \partial M_{T,H} dH = -\mu_0 \int_0^M \partial H_{T,M} dM. \tag{4}$$

The total entropy S of magnetic materials is defined as the sum of magnetic $S_M(T,H)$, lattice $S_L(T,H)$ and, as a first approximation, field independent electronic $S_E(T)$ entropies [6,33]. If we consider that S remains constant in closed systems in an adiabatic process, an increase in S associated to the magnetic degrees of freedom leads to a decrease in the contribution of S related to the nonmagnetic ones, and *vice versa*. In other words, the magnetic system experiments the aforementioned adiabatic temperature change ΔT_{ad} when the magnetic field changes in order to keep constant the total entropy S, or equivalently, in an adiabatic process the variation of H entails the variation of T, what has been denoted as $T(H)$ in Eq. (1).

Taking into account that the heat capacity $C = \partial E/\partial T$ is a measurement of how a system absorbs energy E and distributes it between its different degrees of freedom in order to increase the temperature T, the physical meaning of the magnetocaloric parameter ξ_S is given, as H and T vary, by the ratio of the temperature variation of the magnetic energy E_H with respect to C_H, and corresponds to the change in T due to the magnetic degree of freedom. This argument allow us to determine the optimum value of the magnetocaloric effect as $dT_{ad}^{max} = T_C d\xi_S^{max}$, where T_C is the temperature at which the MCE is maximum, resulting $\Delta T_{ad}^{max} = \sqrt{\mu_0 T_C M_{sat} H/C_H}$, according to the result previously reported in the literature [34,35], after considering that the maximum temperature variation of E_H (from saturation magnetization M_{sat} to null one) occurs just in the temperature adiabatic range ΔT_{ad}, i.e., when the MCE occurs. Analogously, from the relationship $dS_{max} = -C_H d\xi_S^{max}$, we can obtain $|\Delta T_{ad}^{max} \Delta S_{max}| = \mu_0 M_{sat} H$ in agreement with the "sum rule" $\eta_{max} = \int_0^\infty \Delta S dT = \int_0^\infty \Delta T_{ad} dS = \mu_0 M_{sat} H$ (in absolute value) [36].

As it was above mentioned, the experimental relevance of ξ_S consists in its relationship with both the reversible adiabatic temperature change $\Delta T_{ad} = T(0)\xi_S$, and the reversible isothermal entropy change $\Delta S = -C_H \xi_S$. The higher the $|\partial M_{T,H}|$ values (as it occurs for the magnetic field H), or smaller the C_H values, the higher the magnetocaloric parameter ξ_S (ΔT_{ad} or ΔS).

The result $T(H) = T(0)$ in Eq. (1), i.e., $\Delta T_{ad} = \Delta S = 0$, means that the MCE vanishes or, at least, is quite weak ($\xi_S = 0$): for very low applied fields, small temperature variation of the magnetization, and very high heat capacity of the magnetocaloric materials. Others several features are required at the same time to guarantee the quality of the material for being employed as a potential refrigerant in a magnetic refrigerator, namely zero magnetic hysteresis and large thermal conductivity to ensure remarkable rapid heat exchange [4].

Eq. (3) distinguishes both the inverse (when $\Delta T_{ad} < 0$) and direct MCE (when $\Delta T_{ad} > 0$) associated respectively with negative and positive values of ξ_S, related in this work with the existing FOPT and SOPT, as it can be seen in the upper and lower panel in Fig. 1. Analogously, Eq. (4) differentiates between the inverse ($\Delta S > 0$) and direct ($\Delta S < 0$) MCE associated with positive and negative sign of $\partial M_{T,H}$, which can also be seen in the upper and lower panels in Fig. 1, respectively. Although the magnetocaloric parameter ξ_S (given in Eq. (2)) has been initially introduced for materials with SOPT's (where M is a state function), its use can be extended to Heusler alloy-type materials with FOPTs. For this kind of materials the temperature derivative of M may present a discontinuity that can be totally rounded due to inhomogeneities, being $\partial M_{T,H}$ continuous in the temperature range where the FOPT takes place [37,38]. However, it is worth noting that this approximation cannot carelessly be extended to phase-separated manganite $Pr_{0.5}Sr_{0.5}MnO_3$ in the temperature range where first-order FM–AFM–FM phase transitions take place [39].

It is important to know that although there exist relationships between ΔT_{ad} and the H-, T- and S-derivatives of M:

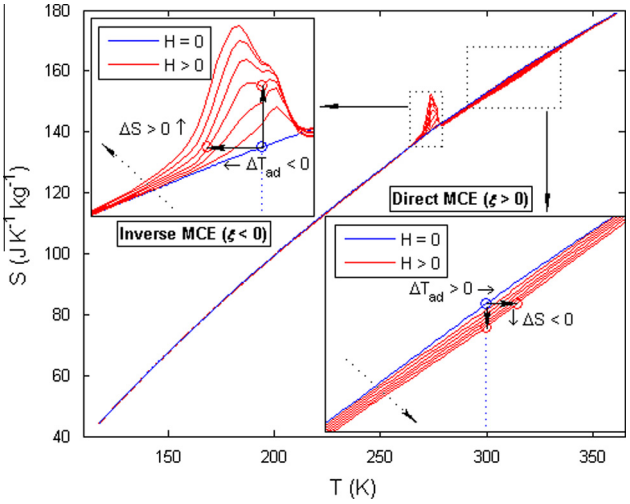

Fig. 1. $S(T,H)$ diagram of the MCE showing the field- and temperature-dependence of the experimental total entropy S for $Ni_{50.29}Mn_{36.47}Sn_{13.24}$ alloy ribbons. The upper and lower insets display a magnification of the inverse and direct MCE, respectively as expanded views of the main panel. The magnetocaloric effect is shown in terms of both ΔS (change in the entropy S as vertical arrows or isothermal process), or in terms of ΔT_{ad} (change in the temperature T as horizontal arrows or adiabatic process), at given temperature T for a magnetic field value H (up to 3 T). Dotted arrows indicate how the magnetic field increases.

$$\Delta T_{ad}(T,H) = -\mu_0 \int_0^H \partial M_{S,H}\, dH = -\mu_0 \int_0^H (\partial M_{H,T} - \partial M_{H,S})/\partial M_{T,H}\, dH, \quad (5)$$

as far as we know, no experimental research has been reported for the indirect determination of ΔT_{ad} based only on magnetization data due, in principle, to its experimental difficulties, as occurs, similarly, for ΔS in the second equality of Eq. (4).

According to the aforementioned description, a change in the magnetic field ΔH produces a change in ΔS associated with the variation of the magnetization related both to the magnetic (spin degrees of freedom) and nonmagnetic (essentially lattice degrees of freedom) subsystems, [32], which can be rewritten for an isothermal process as follows:

$$S(T,H) = S(T,0) + \Delta S(T,H) = \int_0^T (C(T,0)/T)dT + \mu_0 \int_0^H \partial M_{T,H}\, dH, \quad (6)$$

where the differential relation $C(T,0) = T\partial S_T(T,0)$, and the first equality in the Maxwell relationships (given in Eq. (4)) for the total isothermal entropy change ΔS, have been used.

Furthermore, from Eq. (6) the reversible adiabatic temperature change ΔT_{ad} can also be obtained from the numerical resolution of the equation [40–43]:

$$S(T,0) = S(T + \Delta T_{ad}, H) \rightarrow \Delta T_{ad} = [T(S,H) - T(S,0)]_S. \quad (7)$$

In this scenario, one can determine the MCE (ΔS and ΔT_{ad}) in a magnetic material using Eqs. (6) and (7), after measuring the zero-field heat capacity $C(T,0)$ and the isofield $M_H(T)$ magnetization (or the isothermal $M_T(H)$ one for anhysteretic processes).

Taking into account that in magnetic refrigeration magnetocaloric materials follow thermodynamic cycles that, in general, consist of isothermal, isofield or adiabatic irreversible processes, the evaluation of their magnetocaloric response should be carried out in the whole involved processes in order to determine a realistic study of the MCE. In this work both ΔS and ΔT_{ad} have been determined from isofield $M_H(T)$ magnetization heating and cooling measurements (considering thermal hysteresis in the M_{ZFC}, M_{FC} and M_{FH} protocols), and from isothermal $M_T(H)$ ones magnetizing and demagnetizing (taking into account the magnetic hysteresis). In other words, the phase coexistence line $T(H)$ should be crossed by varying one of the control variable (T or H) while the other one is kept constant in materials undergoing FOPT's.

3.2. Thermomagnetic properties

According to the Widom's scaling hypothesis for materials undergoing a SOPT [44], near the critical point (T_C) their free energy $F(\varepsilon,H) = F_r(0,0) + F_s(\varepsilon,H)$ can be written as the sum of a regular part F_r and a singular one F_s, being F_s a generalized homogeneous function, thus the thermodynamic variable $Y(\varepsilon,H)$ (for instance Y = magnetization $M = -\mu_0^{-1}\partial F_{H,T}$, susceptibility $\chi = -\mu_0^{-1}\partial^2 F_{H^2,T}$, entropy $S = -\partial F_{T,H},\ldots$) [45,46], possesses the following power-law dependences in the environment of T_C:

$$Y(0,H) = Y_C(H) = Y(0,1)H^b; \quad \varepsilon = 0, \quad (8)$$

$$Y(\varepsilon,0) = Y_0(\varepsilon) = \begin{cases} Y(1,0)\varepsilon^a & ; \quad \varepsilon \geqslant 0 \\ Y(-1,0)|\varepsilon|^a; & \varepsilon < 0 \end{cases}, \quad (9)$$

where $\varepsilon = (T - T_C)/T_C$ is the reduced temperature, while Y_0 and Y_C are the spontaneous or initial ($H = 0$) and the critical ($\varepsilon = 0$) values, respectively, $Y(0,1)$ and $Y(\pm 1,0)$ are the critical amplitudes, and $a(Y)$ and $b(Y)$ are the critical exponents for each thermodynamic variable Y being independent only two of them. In the literature it is usual refer to these critical exponents as: $a(M) = \beta$ ($\varepsilon < 0$), $b(M) = 1/\delta$, $a(\chi) = -\gamma$, $b(S) = n$, etc., and to obtain the two independent ones from the fit of Eq. (8) and/or following the Kouvel-Fisher iterative method [47], and the remaining ones through the Widom's [44], Griffiths' [48] or Rushbrooke's [49] scaling laws, i.e., relationships between critical exponents.

This hypothesis also allows us to obtain a generalized expression for the equations of state for magnetic systems as:

$$\frac{Y(\varepsilon,H)}{H^b} = \tau\left(\frac{\varepsilon}{H^{1/\Delta}}\right) \rightarrow y_t = \tau(t), \quad (10)$$

$$\frac{Y(\varepsilon,H)}{|\varepsilon|^a} = f_{\pm}\left(\frac{H}{|\varepsilon|^{\Delta}}\right) \rightarrow y_h = f_{\pm}(h), \quad (11)$$

where $y_t = Y/H^b$ is the renormalized temperature dependence of the thermodynamic variable Y (m_t for the magnetization M [39,50]), $t = \varepsilon/H^{1/\Delta}$ the renormalized temperature, τ the temperature scaling function, $y_h = Y/|\varepsilon|^a$ the Y renormalized field dependence (m_h for the magnetization M [39,50] or j_h for the susceptibility χ [39]), $h = H/|\varepsilon|^{\Delta}$ the renormalized field, f_+ (for $T > T_C$) and f_- (for $T < T_C$) the field scaling functions, and $\Delta = a/b$ the so-called gap exponent or the Widom's scaling law. Eqs. (10) and (11) are usually presented in the literature for $Y = M$ [48].

According to Eqs. (10) and (11), if appropriate values of the critical exponents a and b, and T_C are used to plot y_t *vs.* t, or y_h *vs.* h, all experimental data points will collapse, respectively, onto one universal curve τ, or two universal ones: f_+ (for $T > T_C$) and f_- (for $T < T_C$). This is an important criterion to validate the reliability of the procedure used to obtain the critical exponents and will be used in this work for $Y = M$.

4. Results and discussion

Fig. 2 shows the X-ray diffraction patterns of the $Ni_{50.29}Mn_{36.47}Sn_{13.24}$ ribbons at 340 K (upper panel) and 100 K (lower panel). The XRD pattern carried out at 340 K above the magnetic phase transition at T_{CA} (upper panel), confirms that the phase present in the studied sample is a pure AP. The appearance of the super-lattice reflections with the Miller indices (1 1 1) and (3 1 1) suggest that the studied alloy is crystallized in the highly ordered cubic $L2_1$ Heusler structure, with lattice parameter $a_A = 0.59848(3)$ nm and unit cell volume $v_A = 0.21436(3)$ nm^3. On the other hand, at the temperature of 100 K below the magnetic phase transition at T_{CM} (lower panel), the XRD pattern indicates a phase coexistence of the mentioned cubic $L2_1$ structure together with the monoclinic one corresponding to the MP. The new formed monoclinic structure of the MP shows a fourteen-layer modulation (14 M) with the lattice parameters: $a_M = 0.4408(7)$ nm, $b_M = 0.5673(5)$ nm, $c_M = 3.0033(1)$ nm, $\alpha = 93.81°$ and unit cell volume $v_M = 0.107(1)$ nm^3. A change in the sample dimensions will occur during the magnetostructural phase transition provided that a noticeable difference between the volumes of the unit cells of the AP and MP ($\delta v = v_M - v_A$) exists (data collected in Table 1 together with the main experimental results of this work). Accurate determinations in Ni–Mn–Sn Heusler alloy ribbons of the austenitic and martensitic structures from neutron diffraction experiments have confirmed a ~0.5% relative volume change [16,51].

This AP–MP phase coexistence that appears below the magnetostructural transition at T_{str} is a consequence of the nature of the FOPT and can be extended above T_{str} as it is confirmed by numerous experiments [22], thus there exists phase coexistence of the MP having a secondary AP with spontaneous magnetization M_{0A} ($T < T_{str}$), and in the same sense that of AP having a secondary MP with spontaneous magnetization M_{0M} ($T > T_{str}$), in the temperature and field limits that will be specified below.

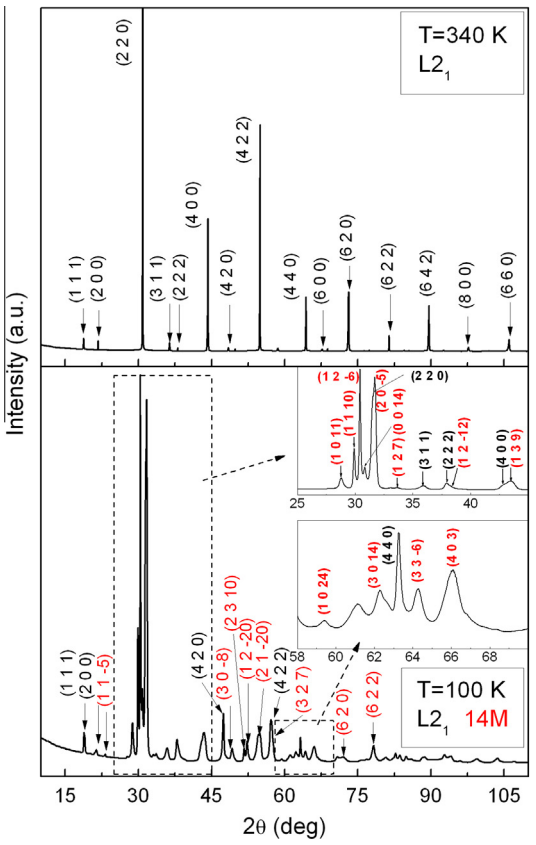

Fig. 2. X-ray diffraction patterns for the as-quenched ribbons measured at 340 K (upper panel) and 100 K (lower panel). The insets show details to clarify the prominent peaks in the range $10° \leqslant 2\theta \leqslant 110°$. In the lower panel Miller indices typed in black and red correspond to the $L2_1$ and 14 M crystal structures, respectively. (For interpretation of the references to color in this figure legend, the reader is referred to the web version of this article.)

As it was also mentioned above, the Mn excess x together with the volume change in the unit cell of the MP ($\delta v < 0$), make the existing FM coupling in the AP that is located in the environment of the Mn ions, transforms to AFM coupling in the MP located both in the surroundings of the Mn ions at the Mn and Sn sites [23,24].

Fig. 3 represents the ZFC, FC and FH temperature dependences of the specific magnetization $\sigma_H(T)$ recorded from 50 K to 400 K at 5 mT (panel a), 10 mT and 20 mT (b), 30 mT, 60 mT and 0.5 T (c), and 1 T (d). It can be distinguished that the studied sample experiments four times the existing phase transitions: two times cooling in a zero-field (ZFC$^-$) and nonzero-field (FC) states, and two times heating with applied fields (ZFC and FH). These experimental data exhibit some common features associated with this kind of Ni–Mn–Z Heusler alloys, such as:

(i) First-order magneto-structural phase transition (MP ↔ AP) at temperature T_{str} (upward triangles on heating and downward triangles on cooling, determined from the corresponding inflection points of $\sigma_H(T)$), known as (←) the Martensitic transformation from the high-temperature AP to the low-temperature MP with lower symmetry.

(ii) An overheating (undercooling) is required to transform MP → AP (MP ← AP) resulting in a field-dependent δT-width thermal hysteresis loop in the σ_H *vs.* T curves. This thermal hysteresis value, $\delta T = 17.0(5)$ K, becomes field independent for a high enough critical magnetic field value H_R (panels 3c and 3d). The meaning of this magnetic field H_R will be specified below.

(iii) The experimental $\sigma_H(T)$ data displayed in Fig. 3 present a strong magnetization change $\delta\sigma = \sigma_M - \sigma_A < 0$ at the temperature T_{str}, where σ_M and σ_A are the magnetization values corresponding to the MP and AP, respectively. Although this change is attributed to the Martensitic transformation at temperature T_{str}, it takes place, as it is usually referred in the literature [52], over the temperature range given by the characteristic temperatures of the Martensitic transformation: (←) martensite start $M_S = 256.7(5)$ K, martensite finish $M_F = 244.7(5)$ K, and (→) austenite start $A_S = 258.3(5)$ K and austenite finish $A_F = 274.8(5)$ K, defined as the extreme values of $\sigma_H(T)$ and marked as solid symbols ● in panel 3d for a magnetic field value higher than H_R.

In this scenario, displaying the MP (monoclinic) and AP (cubic, with higher crystalline symmetry and less effective anisotropy) phase coexistence with AFM and FM orderings, respectively, the studied sample can be treated, in the simplest case, via two magnetic phases with opposite-aligned magnetic moments. Therefore, in addition to the magnetic anisotropies present in a single phase, a significant initial magnetic permeability μ variation can be introduced due to the induced anisotropy by the secondary phase with different magnetic order, i.e., secondary AP with FM ordering and spontaneous magnetization M_{0A} ($>M_{0M}$) in the parent MP ($T < T_{str}$), and *vice versa*, MP with AFM ordering and lower spontaneous magnetization value in the AP ($T > T_{str}$).

According to the so-called Hopkinson effect [53], the initial permeability μ of many ferromagnetic materials can increase with increasing temperature due to the influence of the effective magnetic anisotropy induced by the secondary phase, and exhibiting a sharp peak below the critical temperature T_C followed by a drop to a small value. In others words, when the temperature approaches to T_C the decrease rate of the induced effective anisotropy energy density (e_A) (that prevents the alignment of the magnetization with the field) is much faster than that magnetic energy density (e_H) (with the opposite result), and therefore the following magnetic orderings can take place: (i) (↑↓) opposite-aligned magnetic moments in both phases with net opposite component M (↓) with H (↑) (when $e_A > e_H$); (ii) (↑↓) opposite-aligned magnetic moments with null magnetization M at T_{cp} (when the opposite aligned driving forces are compensated $e_A = e_H$); and, (iii) (↑↑) parallel alignment of magnetic moments with local maximum of the $\sigma_H(T)$ curves or an abrupt change in its temperature derivative at T_R (when $e_A = 0$).

For the sake of best understanding, if the magnetic field H is kept constant and the temperature increases (namely the ZFC protocol), the opposite magnetic moments of the two phases (when $e_A > e_H$) start to rotate from their initial directions (↑↓) towards the direction of the applied magnetic field. As a result, at the so-called compensate point T_{cp} both magnetic moments compensate each other (↑↓) (open symbols ○ in panels 3a, 3b and 3c, where $\sigma_{ZFC}(T_{cp}, H) = 0$, $\mu(T_{cp}, H) = 0$ and $e_A = e_H$) [38,54,55], and at the so-called spin reorientation temperature T_R they become parallel (↑↑) to the applied magnetic field when $e_A = 0$ [27] (solid symbols ■ in panels 3a, 3b and 3c with a local maximum of the $\sigma_{ZFC}(T)$ curves for $T < T_{str}$, or an abrupt change in its temperature derivative for $T > T_{str}$, that specify the temperature metastability limits).

Analogously, in terms of the magnetic energy, if the temperature T is kept fixed and the magnetic field is increased, the opposite magnetic moments of the two phases start to rotate from the easy magnetization axis towards the direction of the applied magnetic field. At the so-called compensate field H_{cp} (where $\sigma_{ZFC}(T,H_{cp}) = 0$, $\mu(T,H_{cp}) = 0$ and $e_A = e_H$), these two sublattice magnetic moments cancel each other and at a given critical magnetic field, called the spin reorientation magnetic field H_R, they become parallel aligned with the applied magnetic field direction when $e_A = 0$.

Table 1
Summary of the main experimental results obtained in this work for the studied $Ni_{50.29}Mn_{36.47}Sn_{13.24}$ alloy ribbons related to the Martensite phase (MP), Austenite phase (AP) and Martensitic transformation (MP ↔ AP). CA = critical amplitudes, HL = magnetic hysteretic losses.

		MP	MP ↔ AP	AP
Lattice parameters (nm)	a_M	0.4408(7)		
	b_M	0.5673(5)		
	c_M	3.0033(1)		
	α (°)	93.81		
	a_A			0.59848(3)
Vol. unit cell (nm^3)	v	0.107(1)		0.21436(3)
	$\lvert\delta v\rvert$		0.107(1)	
$\delta T \pm 0.5$ (K) ($H > H_R$)			17.0	
$\lvert\delta\sigma\rvert$ (emu g^{-1}) ($H > H_R$)	ZFC, FH		21	
	FC		25	
Characteristic temperatures ±0.5 (K) ($\mu_0 H$ = 1 T)	M_S	256.7		
	M_F	244.7		
	A_S			258.3
	A_F			274.8
CA (emu g^{-1})	$\sigma(-1,0)$	36.3(7)		96(1)
$\sigma_{ZFC}(T_R,H_R)$ (emu g^{-1})	$\sigma_{ZFC}(-1,0)$			
	φ	0.60(1)		
$T_C \pm 0.5$ (K)	ZFC	252.7		311.7
	$C(T,0)$			311.2
$T_{cp} \pm 0.5$ (K)	$\mu_0 H_{cp}$ = 5 mT	226.6		
	$\mu_0 H_{cp}$ = 60 mT	60.2		
$T_R \pm 0.5$ (K)	$\mu_0 H_R$ = 5 mT	244.3		
	$\mu_0 H_R$ = 0.5 T	60.8		
T_{str} (K) (→)	$\mu_0 H$ = 20 mT		273.2(5)	
	$\mu_0 H$ = 3 T		269.2(5)	
	P1		270(1)	
	P2		272(1)	
	C(T,0)		271.1(5)	
HL ± 0.1 (J kg^{-1})	T_{str}(P1)		11.8	
	T_{str}(P2)		19.9	
$\Delta S_{pk} \pm 0.1$ (J K^{-1} kg^{-1}) ($\mu_0 H$ = 3 T) [S(0,1) (J K^{-1} kg^{-1}), n]	ZFC (FH)		11.8	−2.2 [1.03(2), 0.70(1)]
	FC		17.3	
	$T_0 H\uparrow$ (P1)		11.9 [4.41(1), 0.927(2)]	
	$T_0 H\downarrow$ (P1)		12.0 [4.395(1), 0.936(1)]	
	$T_0 H\uparrow$ (P2)		12.0 [4.62(1), 0.904(3)]	
	$T_0 H\downarrow$ (P2)		13.4 [4.844(5), 0.935(1)]	
$\Delta T_{ad} \pm 0.1$ (K) [ΔT_{ad}(0,1) (K), θ]	ZFC		−6.3	4.7 [2.28(2), 0.68(2)]
	FC		−6.6	
Critical exponents	n			0.70(1)
	β			0.48(4)
	$1/\delta$			0.28(1)
	Δ			1.74(1)

It is worth pointing out that, the higher the magnetic field intensity the smaller T_{cp} (↑↓) and T_R (↑↑) values (with $T_{cp} < T_R$). The magenta line in panel 3c confirms this decreasing field-evolution of T_R through the fitting of the local maximum of the $\sigma_{ZFC}(T)$ curves for $T < T_{str}$, as a power-law of the reduced temperature $\varepsilon = (T_R - T_{CM})/T_{CM} < 0$ according to the expression $\sigma_{ZFC}(T_R, H_R) = \sigma_{ZFC}(-1,0)|\varepsilon|^{\varphi}$, with the fitting parameters: $\sigma_{ZFC}(-1,0)$ = 36.3(7) A m^2 kg^{-1}, φ = 0.60(1), where T_{CM} = 252.7(5) K (cross symbols × in panels 3a and 3c determined from the inflection points of $\sigma_{ZFC}(T)$ at low field $\mu_0 H$ = 5 mT). This result is physically expected, since the increase of the magnetic field intensity reduces the induced effective magnetic anisotropy energy, so a smaller amount of thermal energy density (e_T) will be required to make rotate the magnetization towards the direction of the applied magnetic field [27]. The parameter $\sigma_{ZFC}(-1,0)$ determined from this fit gives, as a first approximation, the magnetization in the MP at T = 0 K when an applied magnetic field H_R overcome the induced effective magnetic anisotropy by the secondary AP, i.e., this parameter corresponds to the critical amplitude of the *spontaneous magnetization* $\sigma_M(-1,0)$ in the MP beyond the metastability range defined by the $T_R(H_R)$ phase coexistence line. Because of the high-field induced nature of the FM state in the MP, the validity of the term *spontaneous magnetization* is questionable. Nevertheless, it may be of great interest to note that there are neither theoretical predictions nor experimental method to obtain the spontaneous magnetization in multiphase systems with, at least, three phase transitions.

The decreasing field-evolution of T_R (↑↑) for $T > T_{str}$ can be seen by the green line (guide to the eyes), where T_{CA} = 311.7(5) K (cross symbols ×). The corresponding decrease of the compensate point T_{cp} (↑↓), with $T_{cp} < T_R < T_{CM}$, can be visualized following the open symbols ○ throughout Fig. 3 as the magnetic field increases.

According to these arguments (similarly to diamagnetic phenomenology and, therefore, named in the literature as Quasy-Diamagnetic-like (QD) behavior [55]), a negative value (↑↓) of the initial permeability μ can be obtained due to a strong induced effective anisotropy ($e_A > e_H$) in the temperature range below the compensate point $T_{cp}(H)$ with $H < H_{cp}$. This QD-like behavior has been observed to appear from T_{cp} = 226.6(5) K at $\mu_0 H$ = 5 mT, and decreases down to T_{cp} = 60.2(5) K for $\mu_0 H$ = 60 mT, due to the equipment limitations we are not able to measure this feature at temperatures lower than 50 K.

On the other hand, a spin reorientation temperature $T_R(H)$ has been observed from T_R = 244.3(5) K (T_R = 60.8(5) K) when the sample is magnetized with the critical magnetic field value $\mu_0 H_R$ = 5 mT ($\mu_0 H_R$ = 0.5 T). At higher magnetic field values the magnetic moments of the two sublattice become parallel to the applied magnetic field and, once it happens, the AFM order in the MP changes

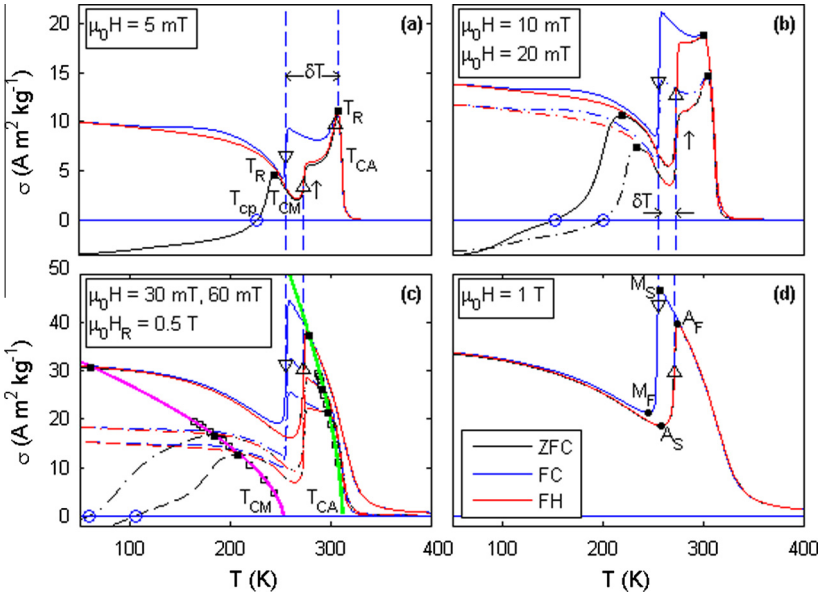

Fig. 3. ZFC, FC and FH temperature dependence of the specific magnetization $\sigma_H(T)$ measured at $H = 5$ mT (a), $H = 10$ mT (dash-dotted lines) and $H = 20$ mT (solid lines) (b), $H = 30$ mT (dashed lines), $H = 60$ mT (dash-dotted lines) and $H_R = 0.5$ T (solid lines) (c) and $H = 1$ T (d). In panel c we mark with solid symbols ■ the local maximum of the displayed $\sigma_{ZFC}(T)$ curves at the indicated magnetic field values, and with open symbols □ the corresponding local maximum of the not shown $\sigma_{ZFC}(T)$ curves. The meaning of the nomenclatures and the other symbols is cited in the text.

to FM one, the ZFC and FH curves become coincident, the induced effective anisotropy energy density is null $e_A = 0$, and the Hopkinson effect and the metastability range disappear (panel 3d).

On increasing the temperature (→), Fig. 3a (two upward triangles) and 3b show a two-step magneto-structural transformation since the applied field (or e_H) at T_{str} is not strong enough to drive the phase transition (first step) and, therefore, an extra contribution of the thermal energy e_T is required (second step at higher temperature). As the magnetic field increases (vertical arrows ↑ in panels 3a and 3b), e_H becomes high enough to drive the magneto-structural phase transition at T_{str}.

The complete T- and H-dependence of $\sigma_H(T)$ using both the ZFC (similarly to FH for $H > H_R$) and FC protocols have been shown in Fig. 4a and b, respectively. As it is can be seen, the magnetostructural phase transition at $T_{str} = 271(2)$ K introduces a jump in the magnetization $\delta\sigma_{ZFC} \approx 21$ A m^2 kg^{-1} and $\delta\sigma_{FC} \approx 25$ A m^2 kg^{-1} (for $H > H_R$), or, equivalently, an increase in $\partial\sigma_{T,H}$ with the concomitant enhancement of the magnetocaloric parameter ξ_S (Eq. (2)). Fig. 4a shows for the ZFC process, in the low temperature ($T < T_R$) and low field ($H < H_R$) ranges, the influence of the induced effective anisotropy on the magnetization of the metastable MP–AP phase coexistence, and how it disappears in the FC process (Fig. 4b), making the splitting between both ZFC–FC curves to occur.

To further characterize the magnetic properties of the studied sample, the field dependence of the specific magnetization $\sigma_T(H)$ was measured around the magnetostructural phase transition by using the P1 and P2 protocols in the temperature range defined through the characteristic A_S and A_F temperatures, obtaining the following behavior: for $T < A_S$, high-field magnetization decreases gradually with increasing temperature as T_{CM} is approached; in the temperature range from A_S to A_F, however, besides a sharp increase in the magnetization, a sudden change of slope can be observed in the $\sigma_T(H)$ curves around 2.5 T, which is associated with the magneto-structural transition (Fig. 5 in the P1 protocol); and finally, at higher temperatures $T > A_F$, the latter magnetic behavior disappears and magnetization decreases with increasing temperature as T_{CA} is approached.

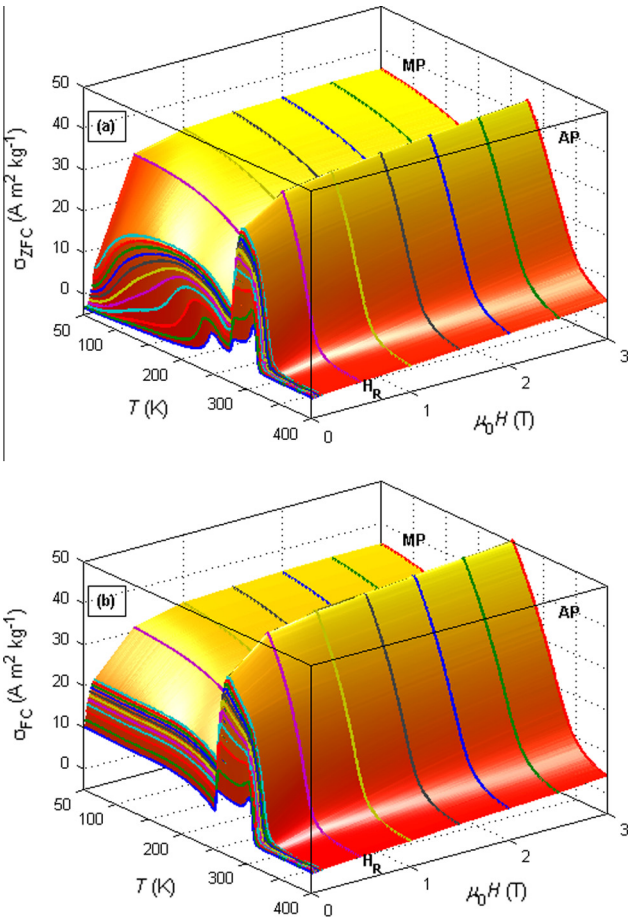

Fig. 4. ZFC – similarly to FH for $H > H_R$ (a) and FC (b) temperature (from 50 K to 400 K) and field (up to 3 T) dependences of the specific magnetization $\sigma(T,H)$. Solid lines correspond to the experimental isofield measurements.

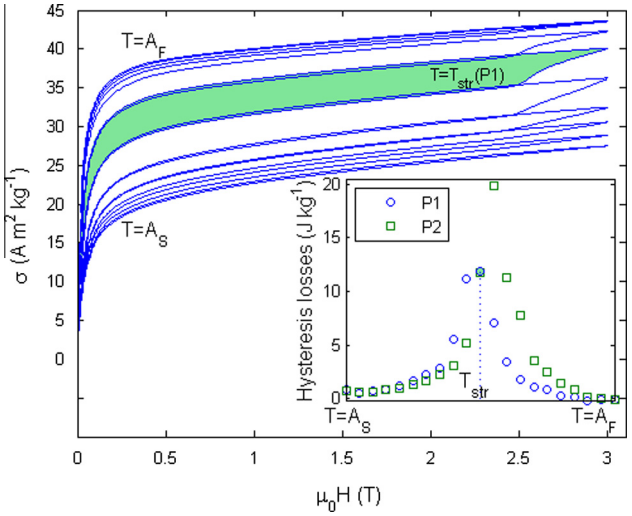

Fig. 5. Isothermal field dependence of the specific magnetization $\sigma_T(H)$ measured around the magneto-structural phase transition at T_{str} using the P1 protocol. Inset: Magnetic hysteresis losses after using the P1 and P2 protocols showing the correlation between thermal and magnetic hystereses. Filled areas in the main panel and in the inset are linked.

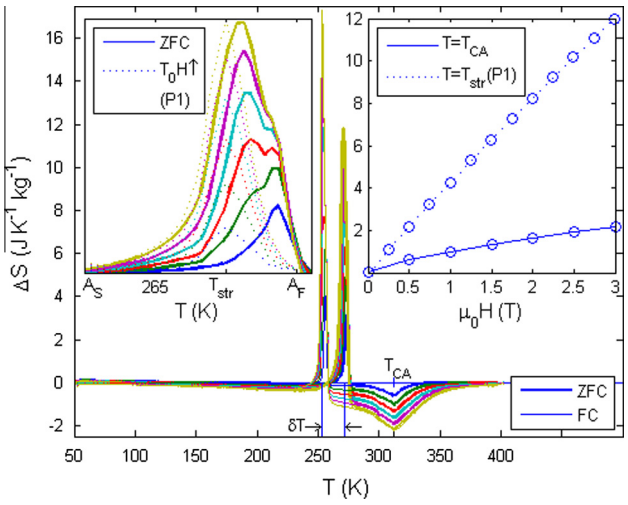

Fig. 6. ZFC (similarly to FH for $H > H_R$) and FC temperature dependences of the isothermal entropy change ΔS recorded at different values of the magnetic field (those marked in the H-axis right inset). Left inset: comparison of the ΔS *vs.* T representations obtained from ZFC and $T_0H\uparrow$ (P1) processes. Right inset: ΔS_{pk} *vs.* H representation (open symbols ○) obtained as a cross section of the ZFC and $T_0H\uparrow$ curves at the temperatures T_{CA} (main panel) and T_{str}(P1) (left inset), respectively. Dotted and solid lines correspond to the fits according to the expression $\Delta S_{pk}(H) = S(0,1)\hat{H}^n - S(0,0)$. Both y-axes in insets are correlated.

Inset in Fig. 5 displays the temperature dependence of the magnetic hysteresis losses when the P1 and P2 protocols have been performed. These values have been calculated as the filled area between the isothermal magnetization and demagnetization curves, in the corresponding temperature range from A_S to A_F, displaying a maximum value at the T_{str}(P1) = 270(1) K and T_{str}(P2) = 272(1) K, and almost zero magnetic hysteresis values outside this temperature range. These hysteretic losses exhibit a complex dependence on both T and H, i.e., magnetic and thermal hystereses are correlated or, in other words, the magnetic hysteresis depends on the thermal history and *vice versa*, which should be carefully subtracted from any thermodynamic variable Y, for instance the refrigerant capacity η of the magnetocaloric materials, in order to obtain the reversible Y value.

To evaluate the MCE we have proceeded with the calculation of $\Delta S(T,H)$ values using the first equality of Eq. (4) in the experimental temperature range from 50 K to 400 K by heating (ZFC and FH) and cooling (FC) the ribbon sample at constant field value, and in the temperature range from A_S to A_F (where the magnetic hysteresis are significant) by magnetizing up to 3 T (denoted as $T_0H\uparrow$ process) or demagnetizing ($T_0H\downarrow$) at constant temperature T_0.

Fig. 6 shows the ZFC (similarly to FH for $H > H_R$) temperature dependence of the ΔS curves obtained under different applied fields $\mu_0H_R = 0.5\ \text{T} < \mu_0H < 3\ \text{T}$ from the $\sigma_{ZFC}(T)$ values presented in Fig. 4a, indicating the existence of the inverse ($A_S < T < A_F$) and direct ($T < A_S$ and $T > A_F$) MCE with remarkable maximum $\Delta S_{pk} = 11.8(1)\ \text{J K}^{-1}\ \text{kg}^{-1}$ and minimum $\Delta S_{pk} = -2.2(1)\ \text{J K}^{-1}\ \text{kg}^{-1}$ values, respectively reached at the maximum applied field of 3 T. A slight field dependence of the positive $T_{pk}(H)$ peak towards lower temperatures has been observed, which is due to the thermodynamic equivalence of T and H as driving forces for the Martensitic transformation. However, the negative peak does not shift and takes place at T_{CA}. The ΔS curve has a tick-like shape, characteristic of a second order phase transition, with the positive λ-peak "embedded" inside the curve due to the inverse MCE.

Together with the ZFC (or FH) magnetocaloric response, Fig. 6 also displays the corresponding FC temperature dependence of the ΔS obtained under different applied fields ($H > H_R$) from the $\sigma_{FC}(T)$ values presented in Fig. 4b, indicating the aforementioned field-independent thermal hysteresis δT and, likewise, the existence of the inverse ($M_F < T < M_S$) and direct ($T < M_F$ and $T > M_S$) MCE with a higher maximum value $\Delta S_{pk} = 17.3(1)\ \text{J K}^{-1}\text{-kg}^{-1}$ for an applied magnetic field of 3 T, exhibiting a similar field evolution of the positive peak towards lower temperatures and the same direct magnetocaloric behavior.

Once the ΔS values have been determined from isofield $\sigma_H(T)$ magnetization (under heating and cooling), its determination from the isothermal $\sigma_T(H)$ curves (by magnetizing and demagnetizing in the P1 and P2 protocols) completes the study of the magnetocaloric response of the $Ni_{50.29}Mn_{36.47}Sn_{13.24}$ alloy ribbons. The comparison of the results obtained from ZFC and $T_0H\uparrow$ in the P1 protocol is shown in the left inset of Fig. 6. It is important to know that there is no shift of the positive peak in the $T_0H\uparrow$ protocol since the e_T is kept constant, contrary to the ZFC where the required e_T decreases as the e_H increases and, consequently, the Martensitic transformation temperature T_{str} shifts towards lower temperatures.

In order to make easy the comparison between these experimental results with those reported in the literature, the field dependences of ΔS_{pk} obtained at the temperature T_{pk} of the positive ($T_{pk} = T_{str}(P_1)$) and negative ($T_{pk} = T_{CA}$) peaks of the ΔS *vs.* T representation, have been fitted according to the modified expression[1] $\Delta S_{pk}(H) = S(0,1)\hat{H}^n - S(0,0)$ [56–58], as it is shown in the right inset of Fig. 6. The latter expression corresponds to Eq. (8) with $Y = S$, where $S(0,0)$ is the contribution of the zero-field entropy $S(T,0)$ at T_{pk}, with n field independent at this temperature. This fitting procedure was carried out in an external magnetic field range from 0 to 3 T with the following parameters $S(0,1) = 1.03(2)\ \text{J K}^{-1}\ \text{kg}^{-1}$, $n = 0.70(1)$, $S(0,0) = 0.03(1)\ \text{J K}^{-1}\ \text{kg}^{-1}$ and $r = 0.9999$ for $T_{pk} = T_{CA}$ (as it is presented in Table 1 together with those values for $T_{pk} = T_{str}(P1)$).

Left inset of Fig. 7 shows the reduced molar heat capacity at zero field $c = C(T,0)/R$, where $R = 8.314\ \text{J K}^{-1}\text{mol}^{-1}$ is the ideal gases constant. As it can be seen, the experimental heat capacity exhibits two clear λ-type peaks at 271.1(5) K and 311.2(5) K, associated to the magnetostructural (at T_{str}) and magnetic (at T_{CA}) phase transi-

[1] For our purposes is equivalent the use of $\hat{H}$ (normalized by its unit in T) or the dimensionless variable $\hat{h} = \mu_0\mu_B H/(k_B T_{pk})$, where μ_B and k_B are the Bohr-magneton and the Boltzmann constant, respectively.

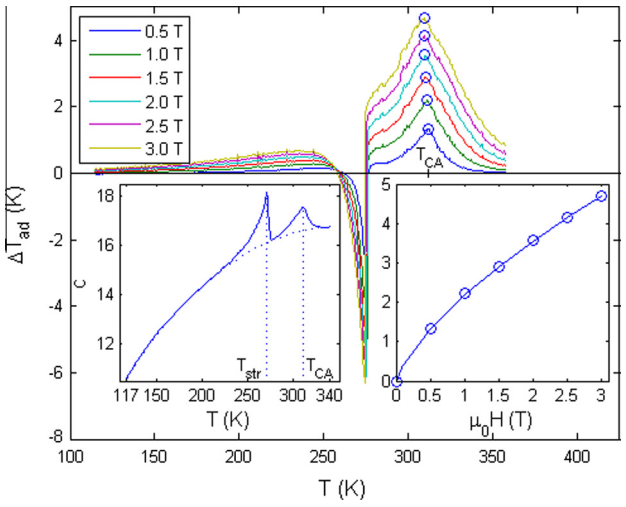

Fig. 7. Temperature dependence of both the magnetocaloric effect ΔT_{ad} recorded at different applied fields (main panel), and that of its reduced molar heat capacity c (left inset). Right inset: ΔT_{ad}^{pk} *vs.* H representation (open symbols ○) obtained as a cross section of the main panel at T_{CA}. Solid line corresponds to the fit according to the expression $\Delta T_{ad}^{pk}(H) = \Delta T_{ad}(0,1)\hat{H}^{\theta}$.

tions, respectively. Dotted line in the inset is a guide to the eyes to roughly visualize the zero-field heat capacities $C_M(T_{pk},0)$ and $C_L(T_{pk},0)$ contributions around both phase transitions, which appropriately obtained would allow us to determine the zero-field entropies contribution $S(0,0)$.

Finally, to fully characterize the MCE in the studied sample, we have calculated the adiabatic temperature change ΔT_{ad} as it is presented in Fig. 7, obtained from the numerical resolution of Eq. (7) once the values of $S(T,0) = \int_0^T (C(T,0)/T)dT$ ([2]blue line in Fig. 1), $\Delta S_{ZFC}(T,H)$ from the first equality of Eq. (4) (Fig. 6), and $S(T,H)$ from Eq. (6) (red lines in Fig. 1) have been previously calculated. The ΔT_{ad} *vs.* T representation, caused by the variation of an external magnetic field from 0 to 3 T, presents the characteristic shape of that to a second order phase transition, like in the ΔS curve, with the negative peak embedded inside due to the inverse MCE, displaying remarkable maximum $\Delta T_{ad}^{pk} = 4.7(1)$ K and minimum $\Delta T_{ad}^{pk} = -6.3(1)$ K values. A field evolution of the positive $T_{pk}(H)$ peak towards lower temperatures has been observed while the negative peak takes place at T_{CA}.

Analogously, the field dependence of ΔT_{ad}^{pk} obtained at the temperature of the positive peak T_{CA} corresponding to the ΔT_{ad} *vs.* T representation, has been fitted according to the power-law $\Delta T_{ad}^{pk}(H) = \Delta T_{ad}(0,1)\hat{H}^{\theta}$ in an external magnetic field range from 0 to 3 T (right inset of Fig. 7), with the fitting parameters $\Delta T_{ad}(0,1) = 2.28(2)$ K, $\theta = 0.68(2)$. Alternatively ΔT_{ad} has been calculated from the numerical resolution of Eq. (3), once the field dependence of the $C(T,H)$ values have been ruled out after considering $C(T,H) \approx C(T,0)$ and assuming that $\Delta T_{ad}/T(0) = |\xi_S| \ll 1$ or, analogously, taking into account the aforementioned first-order approximation $\Delta T_{ad} = -(T/C_H)\Delta S$, showing good agreement between both procedures for the SOPT at T_{CA}, as expected [59].

As it has been previously mentioned, the discontinuities in M and S can be totally rounded due to inhomogeneities, being $\partial M_{T,H}$ and $\partial S_{T,H}$ continuous in the temperature range where the FOPT takes place. Therefore, the discontinuities in M (Fig. 3) and in S (Fig. 1), transform into peaks and can be treated as continuous functions. According to thermodynamics [60], the stability of the equilibrium state places certain conditions on the sign of the thermal, mechanical and chemical response functions. The condition for thermal stability tells us that $C_H > 0$ and $\partial S_{T,H} > 0$. If a small excess of heat is added to a volume element of the Heusler alloy ribbon when the FOPT takes place, then the temperature of the volume element must increase relative to its surroundings so that some of the heat will flow out again. This requires that the heat capacity C_H be positive. If the heat capacity were negative, the temperature would decrease and even more heat would flow in, thus leading to instability. Notice in Fig. 1 that on the right-hand side of the S *vs.* T peak, where the heat capacity $C_H = T\partial S_{T,H}$ is negative, it does not contradict the thermodynamic stability criteria. This negative value of $\partial S_{T,H}$ just indicates that the system is not an equilibrium state in this temperature range, as it has been previously reported in the literature [61].

Since only two of the critical exponents of the SOPT at T_{CA} are independent, in this study we have determined all of them based on these two exponents: $n = 0.70(1)$ obtained from the fitting of the ΔS_{pk} (H) values using Eq. (8) (for $Y = S$ and $b(S) = n$, see right inset of Fig. 6), and the gap exponent $\Delta = 1.74(1)$, obtained according to Eq. (10) from the fitting of reference temperatures as a power-law of the field ($\sim H^{1/\Delta}$), or alternatively, according to Eq. (11) as the fitting of reference fields as a power-law of the temperature ($\sim|\varepsilon|^{\Delta}$) [39,62,63]. Although the determination of $1/\delta$ from Eq. (8) is much faster than that for Δ, this method was not carried out since the value of T_{CA}, as determined from the inflection point of the isofield $\sigma_{ZFC}(T)$ curve at low field, does not coincide exactly with an experimental temperature point of the isothermal $\sigma_T(H)$ measurements, thus quite experimental errors could be introduced. It is also important to note that although ΔT_{ad} (as a temperature magnitude) scales with field as the reduced temperature ε ($\sim H^{1/\Delta}$), the discrepancy found in the values θ and $1/\Delta$ has been explained by means of the experimental procedure undertaken to determine both exponents, in which two samples and two experimental techniques have been used: one sample for the determination of $1/\Delta$ from the magnetization measurement, and the second one to obtain θ from the magnetization and heat capacity measurements, with the subsequent experimental errors introduced in the determination of T_{CA}.

In order to validate the reliability of the critical exponents obtained from this procedure, the temperature and field dependence of the normalized magnetizations σ_t and σ_h (according to the nomenclature used in Eqs. (10) and (11) for $Y = \sigma$, $a(\sigma) = \beta$ and $b(\sigma) = 1/\delta$) has been plotted *vs.* the renormalized temperature t and field h, respectively. It can be observed that the experimental data fall on the universal curve τ in the σ_t *vs.* t representation (main panel of Fig. 8), and on the two universal curves f_+ (for $T > T_{CA}$) and f_- ($T < T_{CA}$) in the $\mathrm{Ln}(\sigma_h)$ *vs.* $\mathrm{Ln}(h)$ representation (inset of Fig. 8). These results satisfactorily indicate that the obtained values of the critical exponents $\beta = 0.48(4)$ for $\varepsilon < 0$, and $1/\delta = 0.28(1)$, using the following relationships:

$$\beta = 1 + n\Delta - \Delta; \quad 1/\delta = 1/\Delta + n - 1, \tag{12}$$

are quite reliable. These values are inside of the range previously reported for the same ribbon sample compositions $Ni_{50}Mn_{25+x}Sn_{25-x}$ with $x = 11$ and $x = 12$ [64].

A relationship between the critical amplitudes $\sigma(0,1)$ and $\sigma(-1,0)$, and the values of the temperature and field scaling functions for $\tau\cdot(t = 0)$ and $f_{\pm}(h = 0)$, respectively, is possible to be determined by combining Eqs. (10) and (11) [39]: $\sigma(0,1) = \tau\cdot(0)$, $f_+(0) = 0$ and $f_-(0) = \sigma(-1,0)$, as has been indicated in Fig. 8, where $\sigma_A(0,1) = 20.0(1)$ A m^2 kg^{-1} T$^{-1/\delta}$ and $\sigma_A(-1,0) = 96(1)$ A m^2 kg^{-1}. Once the $\sigma_A(-1,0)$, T_{CA} and β values are known, the theoretical results of the spontaneous magnetization $\sigma_A(T,0) = \sigma_{0A}(T)$ of the AP, offered by Eq. (9), have been presented in the main panel of Fig. 9 (solid line).

[2] For interpretation of color in Fig. 1, the reader is referred to the web version of this article.

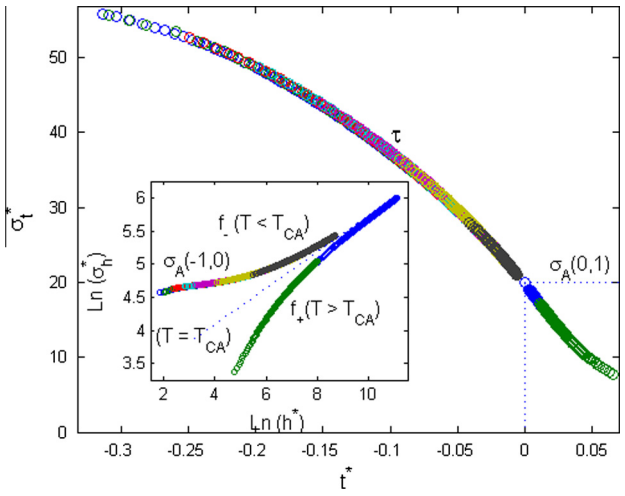

Fig. 8. Universal temperature t or field h dependences of the renormalized σ_t (main panel) and σ_h (inset) magnetizations around the critical point of the SOPT at T_{CA}. σ_t^*, σ_h^*, t^* and h^* are the corresponding dimensionless magnitudes obtained after normalizing by their units.

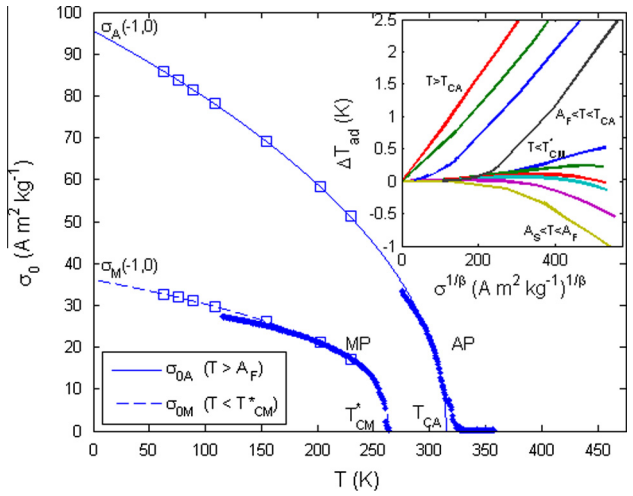

Fig. 9. Temperature dependence below T_{CA} of the experimental spontaneous magnetization σ_0 (dot symbols), along with the theoretical ones offered by Eq. (9) for $T < T_{CA}$ (solid line). Dashed line corresponds to the fitting of *spontaneous magnetization* of the MP according to Eq. (9) for $T < T_{CM}$. Open symbols □ indicate the spontaneous magnetizations at the compensate points T_{cp}. Inset: Isotherms of the ΔT_{ad} change *vs.* the experimental magnetization as $\sigma^{1/\beta}$ at selected temperatures ($T < T_{CM}$, $A_S < T < A_F$, $A_F < T < T_{CA}$ and $T > T_{CA}$).

According to the mean field theory ($\beta = 0.5$) it can be shown that, below the Curie temperature T_C (for our purposes T_{CA} or T_{CM}), the magnetocaloric ΔT_{ad} change is given by [65]:

$$\Delta T_{ad}(T,H) = \frac{N\rho}{2c_\sigma}[\sigma^{1/\beta}(T,H) - \sigma_0^{1/\beta}(T)], \tag{13}$$

where N is the molecular field constant, ρ the density and c_σ the specific heat at constant magnetization. Extrapolating the linear behavior of the MCE effect against the experimental magnetization as $\sigma^{1/\beta}$, gives the slope and interception on the $\sigma^{1/\beta}$-axis which are related to the molecular field constant N and the experimental spontaneous magnetization $\sigma_0(T)$, respectively.

Inset of Fig. 9 displays the magnetocaloric effect as a function of $\sigma^{1/\beta}$ at selected temperatures ($T < T_{CM}$, $A_S < T < A_F$, $A_F < T < T_{CA}$ and $T > T_{CA}$), showing the expected linear dependence in magnetic fields above H_R. Some of the ΔT_{ad} vs. $\sigma^{1/\beta}$ curves, in the temperature range $A_S < T < A_F$ where the magnetostructural phase transition takes place, appear to exhibit two linear regions, but without having field-dependent specific heat data, a complete quantitative analysis of this phenomena is not possible. Further studies are being undertaken without making reference to the mean field model approximation.

The spontaneous magnetization obtained from the inset of Fig. 9 by extrapolation of the linear behavior of the curves in the temperature range $T > A_F$ (AP) is plotted as a function of temperature in the main panel of Fig. 9 (dot symbols), showing a quite good agreement with the theoretical values obtained from Eq. (9) for the SOPT at T_{CA}. Furthermore, although it is not allowed the determination of the critical exponents for the SOPT at T_{CM} and, therefore, to obtain their corresponding universal curves τ and $f_\pm$ (see Fig. 8 for the SOPT at T_{CA}), the linear extrapolation of these curves in the inset of Fig. 9 have also been plotted as a function of the temperature in the temperature range $T < T_{CM}$ (MP), shown with dot symbols in Fig. 9. The obtained Curie temperature value is $T^*_{CM} = 263.2(5)$ K (higher than T_{CM}), and the *spontaneous magnetization* has been fitted according to Eq. (9) ($\varepsilon < 0$) with the critical amplitude $\sigma_M(-1,0) = 36.3(7)$ A m^2 kg^{-1}, when the critical exponent β given by the 3D Heisenberg model ($\beta_H = 0.367$) has been imposed (dashed line in Fig. 9).

The latter analysis in terms of the critical exponent β [64], points out the existence of long-range FM order in the AP ($T < T_{CA}$) and short-range FM order in MP ($T < T_{CM}$), consequence of the MP–AP phase coexistence with $\sigma_{0A} > \sigma_{0M}$, even for higher magnetic field values $H > H_R$.

Regarding the aforementioned treatment of two magnetic phases with their magnetic moments opposite-aligned that describes the MP–AP phase coexistence, i.e., secondary AP with FM ordering and spontaneous magnetization σ_{0A} ($>\sigma_{0M}$) in the parent MP with AFM ordering ($T < T_{str}$). The following expression:

$$z_M\sigma_{0M}(T_{cp}) - z_A\sigma_{0A}(T_{cp}) = 0, \tag{14}$$

at the compensate temperature point $T = T_{cp}$ at which the two oppositely-aligned magnetic moments (↑↓) cancel to each other and $e_A = e_H$ (opens symbols □ in Fig. 9), allow us to obtain the fractions $z_M = 0.72(2)$ and $z_A = 1 - z_M = 0.28(2)$ of the both coexisting MP and AP phases, in agreement with the results obtained from the XRD analyses carried out by means of the integrated area of the prominent peaks.

5. Conclusions

In summary, after considering the hysteretic processes in real thermodynamic cycles, the magnetocaloric response of $Ni_{50.29}Mn_{36.47}Sn_{13.24}$ alloy ribbons has been studied in a large temperature range, showing higher values than 1.5 K T^{-1} in the field dependence of ΔT_{ad} around the magnetostructural, at $T_{str} = 271$ K, and magnetic, at $T_{CA} = 311$ K, phase transitions.

The dimensionless Stoner's magnetocaloric parameter ξ_S has turned out to be the natural variable of the phenomena, and has allowed us to express the MCE formulation in a compact way and to relate both the ΔT_{ad} and ΔS magnetocaloric variables. In order to obtain general physical meaning from the universal behaviors of the magnetic properties, a generalized expression for the equations of state for magnetic materials has been introduced as a powerful tool.

The magnetothermal properties into the temperature and field ranges where MP–AP phase coexistence exists has been studied by means of the induced anisotropy by the AP in the parent MP. This metastability has been studied via the two magnetic MP and AP phases with opposite-aligned magnetic moments. Magnetic field values higher than that of the critical value of $\mu_0 H_R = 0.5$ T

produce that the magnetic moments of the two phases become parallel to the applied magnetic field and, once it happens, the magnetic ordering in the MP changes from AFM to FM, the ZFC and FH magnetizations curves become coincident, the induced effective anisotropy energy density is null $e_A = 0$ and the metastability range disappear.

The magnetocaloric response has been studied within the mean field theory, in which the *spontaneous magnetization* M_0 and a short- (in the MP) and long-range ordering (in the AP) beyond the metastability range, together with the fractions $z_M = 0.72(2)$ and $z_A = 0.28(2)$ of the MP and AP phases in the phase coexistence range, have been obtained.

Acknowledgements

This work has been partially supported under Spanish MINECO research project MAT2010-20798-C05-04, MAT2013-48054-C2-2-R, MAT2013-47231-C2-1-P and FEDER funds. R.C.F. acknowledges a Ph.D. contract from FICYT-Principado de Asturias (Project SV-PA-13-ECOEMP-47). W.O.R. acknowledges FAPERJ and CAPES Brazilian agencies for the financial funding. Work at Amirkhanov Institute of Physics of Daghestan Scientific Center was funded by RFBR (Project No. 12-02-96506).

References

[1] E. Warburg, L. Hönig, Ann. Phys. 256 (1883) 814.
[2] A.M. Tishin, Y.I. Spichkin, The Magnetocaloric Effect and Its Applications, Institute of Physics Publishing, Bristol and Philadelphia, 2003.
[3] W.F. Giauque, D.P. MacDougall, Phys. Rev. 43 (1933) 768.
[4] B.F. Yu, Q. Gao, B. Zhang, X.Z. Meng, Z. Chen, Int. J. Refrig. 26 (2003) 622.
[5] E.C. Stoner, Philos. Mag. 19 (1935) 565.
[6] V.K. Pecharsky, K.A. Gschneidner Jr., J. Appl. Phys. 90 (2001) 4614.
[7] J.M. Yeomans, Statistical Mechanics of Phase Transitions, Claredon Press, Oxford, 1992.
[8] K.A. Gschneidner Jr., V.K. Pecharsky, A.O. Tsokol, Rep. Prog. Phys. 68 (2005) 1479.
[9] E. Bruck, J. Phys. D: Appl. Phys. 38 (2005) R381.
[10] R. Caballero-Flores, V. Franco, A. Conde, K.E. Knipling, M.A. Willard, Appl. Phys. Lett. 98 (2011) 102505.
[11] A. Bhattacharyya, A. Thamizhavel, S.K. Dhar, P. Manfrinetti, J. Alloys Comp. 588 (2014) 720.
[12] V.K. Pecharsky, K.A. Gschneidner Jr., Phys. Rev. Lett. 78 (1997) 4494.
[13] O. Tegus, E. Bruck, K.H. Buschow, F.R. De Boer, Nature 415 (2002) 150.
[14] F. Hu, B. Shen, J. Sun, Z. Cheng, G. Rao, X. Zhang, Appl. Phys. Lett. 78 (2001) 3675.
[15] L. Pareti, M. Solzi, F. Albertini, A. Paoluzi, Eur. Phys. J. B 32 (2003) 303.
[16] A. Planes, L.l. Mañosa, M. Acet, J. Phys.: Condens. Matter 21 (2009) 233201.
[17] J.L. Yan, Z.Z. Li, X. Chen, K.W. Zhou, S.X. Shen, H.B. Zhou, J. Alloys Comp. 506 (2010) 516.
[18] S. Chatterjee, S. Giri, S.K. De, S. Majumdar, J. Alloys Comp. 503 (2010) 273.
[19] H.J. Yu, H. Fu, Z.M. Zeng, J.X. Sun, Z.G. Wang, W.L. Zhou, X.T. Zu, J. Alloys Comp. 477 (2009) 732.
[20] E. Sasıoglu, L.M. Sandratskii, P. Bruno, Phys. Rev. B 70 (2004) 024427.
[21] C.L. Tan, Y.W. Huang, X.H. Tian, J.X. Jiang, W. Cai, Appl. Phys. Lett. 100 (2012) 132402.
[22] S.B. Roy, J. Phys.: Condens. Matter 25 (2013) 183201.
[23] T. Krenke, M. Acet, E.F. Wassermann, X. Moya, L. Mañosa, A. Planes, Phys. Rev. B 72 (2005) 014412.
[24] P.J. Shamberger, F.S. Ohuchi, Phys. Rev. B 79 (2009) 144407.
[25] R. Caballero-Flores, V. Franco, A. Conde, L.F. Kiss, J. Appl. Phys. 105 (2009) 07A919.
[26] T.M. Seixas, M.A. Salgueiro da Silva, O.F. de Lima, J. Lopez, H.F. Braun, G. Eska, J. Phys.: Condens. Matter 22 (2010) 136002.
[27] N.A. de Oliveira, P.J. von Ranke, Phys. Rep. 489 (2010) 89.
[28] P. Weiss, Ann. Phys. 17 (1932) 97.
[29] P. Weiss, R. Forrer, Ann. Phys 5 (1926) 153.
[30] P. Debye, Ann. Phys. 81 (1926) 1154.
[31] W.F. Giauque, J. Am. Chem. Soc. 49 (1927) 1864.
[32] T. Mukherjee, S. Michalski, R. Skomski, D.J. Sellmyer, Ch. Binek, Phys. Rev. B 83 (2011) 214413.
[33] V.K. Pecharsky, K.A. Gschneidner Jr., A.O. Pecharsky, A.M. Tishin, Phys. Rev. B 64 (2001) 144406.
[34] V.I. Zverev, A.M. Tishin, M.D. Kuz'min, J. Appl. Phys. 107 (2010) 043907.
[35] K.G. Sandeman, Scripta Mater. 67 (2012) 566.
[36] L.H. Bennett, M.D. McMichael, L.J. Swartzendruber, R.D. Shull, R.E. Watson, J. Magn. Magn. Mater. 104–107 (1992) 1094.
[37] Y. Imry, M. Wortis, Phys. Rev. B 19 (1979) 3580.
[38] R. Caballero-Flores, T. Sánchez, W.O. Rosa, J. García, L. González-Legarreta, D. Serantes, V.M. Prida, L.l. Escoda, J.J. Suñol, B. Hernando, J. Alloys Comp. 545 (2012) 216.
[39] R. Caballero-Flores, N.S. Bingham, M.H. Phan, M.A. Torija, C. Leighton, V. Franco, A. Conde, H. Srikanth, J. Phys.: Condens. Matter 26 (2014) 286001.
[40] V.K. Pecharsky, K.A. Gschneidner Jr., J. Appl. Phys. 86 (1999) 565.
[41] V.K. Sharma, M.K. Chattopadhyay, R. Kumar, T. Ganguli, P. Tiwari, S.B. Roy, J. Phys.: Condens. Matter 19 (2007) 496207.
[42] S. Tencé, E. Gaudin, B. Chevalier, Intermetallics 18 (2010) 1216.
[43] V.A. Chernenko, J.M. Barandiarán, J. Rodríguez Fernández, D.P. Rojas, J. Gutiérrez, P. Lázpita, I. Orue, J. Magn. Magn. Mater. 324 (2012) 3519.
[44] B. Widom, J. Chem. Phys. 43 (1965) 3898.
[45] H.E. Stanley, Introduction to Phase Transitions and Critical Phenomena, Oxford University Press, London, 1971.
[46] M.H. Coopersmith, Phys. Rev. 167 (1968) 478.
[47] J.S. Kouvel, M.E. Fisher, Phys. Rev. 136 (1964) A1626.
[48] R.B. Griffiths, Phys. Rev. 158 (1967) 176.
[49] G.S. Rushbrooke, J. Chem. Phys. 39 (1963) 842.
[50] V. Franco, R. Caballero-Flores, A. Conde, K.E. Knipling, M.A. Willard, J. Appl. Phys. 109 (2011) 07A905.
[51] P.J. Brown, A.P. Gandy, K. Ishida, R. Kainuma, T. Kanomata, K.-U. Neumann, K. Oikawa, B. Ouladdiaf, K.R.A. Ziebeck, J. Phys.: Condens. Matter 18 (2006) 2249.
[52] T. Krenke, M. Acet, E.F. Wassermann, X. Moya, L. Mañosa, A. Planes, Phys. Rev. B 73 (2006) 174413.
[53] J. Hopkinson, Proc. Roy. Soc. 48 (1890) 1.
[54] J. Sólyom, Fundamentals of the Physics of Solids, vol. 1, Springer, Berlin, 2007.
[55] V.N. Prudnikov, A.P. Kazakov, I.S. Titov, Y.a.N. Kovarskii, N.S. Perov, A.B. Granovsky, I. Dubenko, A.K. Pathak, N. Ali, J. Gonzalez, Phys. Solid State 53 (2011) 490.
[56] T.D. Shen, R.B. Schwarz, J.Y. Coulter, J.D. Thompson, J. Appl. Phys. 91 (2002) 5240.
[57] V. Franco, J.S. Blázquez, A. Conde, Appl. Phys. Lett. 89 (2006) 222512.
[58] V. Franco, A. Conde, M.D. Kuz'min, J.M. Romero-Enrique, J. Appl. Phys. 105 (2009) 07A917.
[59] S. Tencé, R. Caballero-Flores, S. Gorsse, E. Gaudin, B. Chevalier, Inorg. Chem. 53 (2014) 6728.
[60] L.E. Reichl, A Modern Course in Statistical Physics, second ed., John Wiley & Sons, Inc., New York, 1997.
[61] J.I. Pérez-Landazábal, V. Recarte, V. Sánchez-Alarcos, S. Kustov, E. Cesari, J. Alloys Comp. 536S (2012) S277.
[62] V. Franco, A. Conde, Int. J. Refrig. 33 (2010) 465.
[63] V. Franco, A. Conde, V. Provenzano, R.D. Shull, J. Magn. Magn. Mater. 322 (2010) 218.
[64] T.-L. Phan, P. Zhang, N.H. Dan, N.H. Yen, P.T. Thanh, T.D. Thanh, M.H. Phan, S.C. Yu, Appl. Phys. Lett. 101 (2012) 212403.
[65] A.C. Hudgins Jr., A.S. Pavlovic, J. Appl. Phys. 36 (1965) 3628.